Molecular thermal engine based on a highly flexible elastic crystal

Hinako Kato,[a] Yoji Horii[a*], Chiharu Watanabe[a], Toshiyuki Sasaki[b], Kouhei Ichiyanagi[b], Mariko Noguchi[c], Hiroki Fujimori[c], Taro Yamamoto[d], Hal Suzuki[d], Yuichi Hirai[e], Takahito Ohmura[e], Keigo Yano[f], Shotaro Hayashi[f,g], and Takashi Kajiwara[a]

Affiliations

a. Graduate School of Humanity and Science, Nara Women's University, Kitauoya-Higashimachi, Nara 630-8506, Japan

b. SPring-8/JASRI, Kouto, Sayo, Hyogo 679-5198, Japan

c. Graduate School of Integrated Basic Sciences, Nihon University, 3-25-40 Sakurajosui, Setagaya-ku, Tokyo 156-8550, Japan

d. Department of Chemistry, Kindai University, 3-4-1 Kowakae, Higashiosaka City, Osaka 577-8502, Japan

e. National Institute for Materials Science (NIMS), 1-1 Namiki, Tsukuba, Japan

f. School of Engineering Science, Kochi University of Technology, 185 Miyanokuchi, Tosayamada, Kami, Kochi 782-8502, Japan

g. FOREST Center, Research Institute, Kochi University of Technology, 185 Miyanokuchi, Tosayamada, Kami, Kochi 782-8502, Japan

Abstract

Materials that exhibit actuation behaviour in response to external stimuli have a wide range of applications owing to their ability to convert input energy into mechanical work.[1–4] Light and chemicals are common sources of input energy.[2,5–8] However, actuation using thermal energy from ambient-temperature sources remains challenging. In this study, we introduce novel elastic crystals composed of dodecylated porphyrin molecules that exhibit high flexibility and deformation in response to temperature changes. When a crystal is loaded with a small weight and positioned between high- and low-temperature heat sources, it exhibited continuous, large, and rapid oscillations. These oscillations persisted for at least 160 h, corresponding to 3.9 million deformation cycles, as long as the temperature difference was maintained. This study presents the first example of a molecular crystal functioning as an engine that can extract kinetic energy from

static and ambient-temperature sources.

Introduction

Materials exhibiting actuation properties in response to external stimuli have been extensively studied owing to their wide range of applications, including soft robotics, the medical industry (artificial muscles and limbs), and energy storage and conversion. Sophisticated material design has led to the development of soft polymer composites exhibiting autonomous locomotion similar to that of living organisms.[1–4] Liquid crystal elastomers exhibit continuous rolling[6,8] and oscillation[7] when exposed to consistent light and temperature. In these examples, mechanical energy is extracted through a nearly constant external field, eliminating the need for the on-off cycling of the light or heat source. Polymer composites are materials that function as external field-response actuators owing to their high flexibility, which enables facile deformation. Recent developments in crystal engineering have revealed the possibility of endowing organic crystals, which were previously considered rigid, with actuation properties.[5,9–15] Elastic crystals that can be reversibly bent like elastomers while maintaining their crystallinity have also been reported;[16] these materials are considered promising materials for highly durable and flexible optoelectronic[17–23] and magnetic devices.[24–27] Reports on elastic crystals exhibiting actuation in response to light,[28–30] chemicals,[31] and temperature[32,33] underscore the diversity of the operating principles of actuators prepared from molecular crystals. However, the extraction of energy from a constant external field, as demonstrated in polymer composites, is rarely observed in organic crystals and remains a challenging endeavour.[34] Most reported crystal-based actuators require fluctuating external fields, such as the on-off cycling of a light source or heater, for continuous motion. The conversion of heat, the lowest grade of energy, into kinetic energy is notably more challenging than the conversion of light owing to the lack of established design criteria for thermal conversion.

To address the gaps in the literature, in this study, we present the first example of a thermal engine based on elastic crystals. When the crystal is loaded with a weight and placed between high (34–37 °C)- and low (~0 °C)-temperature heat sources, it continuously oscillates, indicating that it can extract kinetic energy from the heat sources. The oscillations continued for at least 160 h, corresponding to over 3.9 million cycles of bending and stretching, demonstrating the high durability of the elastic crystal. To the best of our knowledge, this study is the first to report the continuous operation of an organic crystal-based thermal engine under only static temperature differences. Our results highlight the potential applications of organic elastic crystals as actuators

owing to their high-speed responsiveness to external fields and remarkable durability.

Synthesis and characterisation

The dodecylated porphyrin molecule was synthesised by the ester-exchange reaction of 10,15,20-tetrakis(4-methoxycarbonylphenyl) porphyrin H_2(TMCPP) in 1-dodecanol in the presence of a base catalyst (DBU), as depicted in Figure 1a.[27] Crystallisation of the deacylated porphyrin using dichloromethane and ethanol at 40 °C afforded the needle-like elastic crystals (**1**), with a minor amount of brittle block-shaped crystals (**2**). **1** could be bent under a mechanical force and returned to its original shape when the force is released, indicating its elasticity (Figure 1b and Movie 1). The nanoindentation test results for **1** (Figures S3 and S4) revealed a Young's modulus (E_r) and hardness (H) of 1.8(2) and 0.072(3) GPa, respectively. Furthermore, the Young's modulus of **1** upon bending was determined to be 0.13 GPa (Figures S5–S7). These values are lower than those of most organic compounds[35], confirming the high flexibility of **1**.

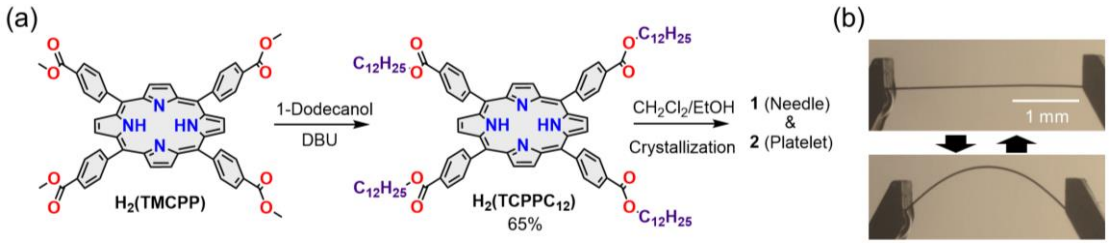

Figure 1. (a) Synthesis and crystallisation of dodecylated porphyrin. (b) Bending of **1**.

Figure 2a summarises the crystal packing of **1** at 298 K. **1** crystallised in the space group *P*-1, and the entire molecule was crystallographically independent. The two dodecyl chains of **1** exhibited heavy disorder at 298 K, as indicated in green, orange, and purple. The porphyrin molecules stacked along the *a*-axis to form a columnar structure surrounded by dodecyl chains. The *a*-axis coincided with the direction of crystal growth. Needle-like crystals with such a one-dimensional molecular arrangement are commonly elastic.[17,36] The intracolumnar distances between porphyrin π-planes (3.67 and 3.82 Å) are longer than that expected for a π–π stacked system (3.3 Å), indicating that the van der Waals interactions between dodecyl chains are the dominant driving force behind the one-dimensional packing of the crystals (Figure S10).

Figure 2b summarises the temperature dependence of the *a*-axis length as a representative parameter. When the temperature was swept from approximately 275 to 223 K, the *a*-axis length gradually increased with the gradual suppression of the disorder on the dodecyl chains (Figure 2c). The crystalline parameters exhibited a similar temperature dependence during the

corresponding heating process, indicating that this process is reversible. Adiabatic and differential scanning calorimetry indicated that the gradual structural changes observed between 275 and 223 K correspond to a second- or higher-order phase transition from the high-temperature (HT) to the low-temperature (LT) phase (see the thermal analysis section in the Supporting Information (SI)). In this paper, the 275–223 K region is referred to as the medium-temperature (MT) state for convenience. The *a*-axis length of **1** increases with decreasing temperature, whereas its *b*-axis length, *c*-axis length, and cell volume decrease. In other words, the needle-like crystals become long and slim upon cooling. The elongation ratio of the crystals associated with the decrease in temperature was observed using optical microscopy (Figure S12 and Table S3). The increase in *a*-axis length correlated with the magnitude of disorder of the dodecyl groups. The heavy thermal motion of the dodecyl chains in the HT phase prevented the porphyrin columns from approaching each other, whereas the suppressed thermal motion of the dodecyl chains upon cooling decreased the intercolumnar distances (Figure 2d). Owing to the chemical pressure from adjacent columns, the intracolumnar molecular distances increased, resulting in an increase in *a*-axis length.

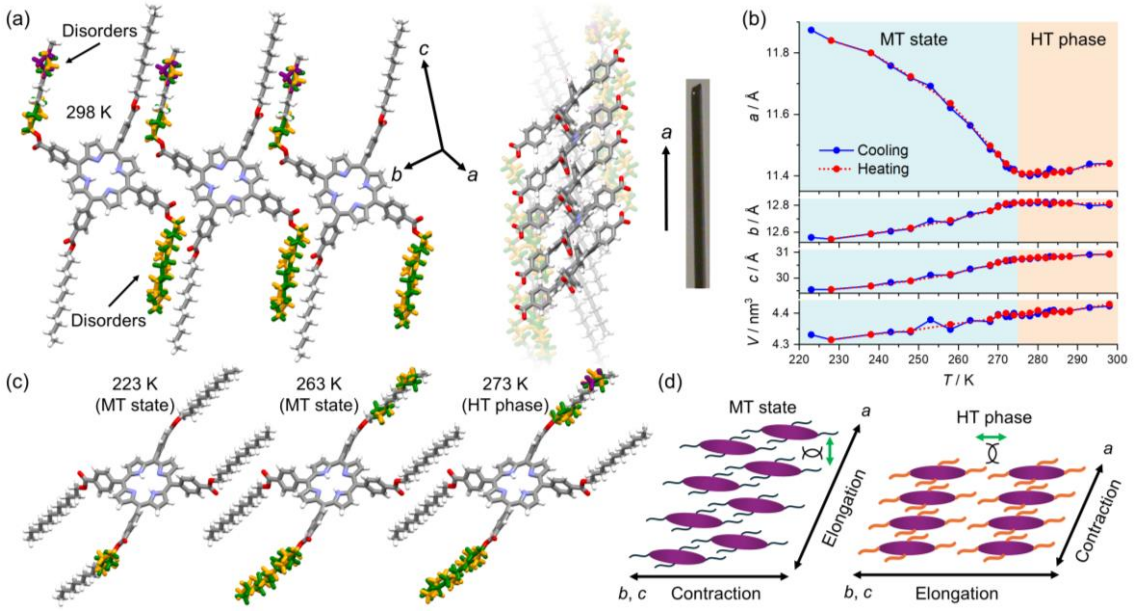

Figure 2. (a) X-ray structures of **1** at 298 K. (b) Temperature dependence of the crystal parameters and (c) X-ray structures of **1**. (d) Schematic illustration of the elongation of the *a*-axis and contraction of the *b*- and *c*-axes upon cooling.

Crystal deformation by changes in temperature

An important consideration in the performance of elastic crystals is their ability to remain flexible at low temperatures.[37,38] Because **1** contains dodecyl chains that exhibit temperature-dependent

thermal motion, its flexibility should depend on the temperature. To briefly examine the temperature dependence of the flexibility of **1**, we attached a weight (1.168 mg of Al) to the tip of **1** (length: 5.7 mm) and cooled the crystal in a refrigerant-free cooling device sealed with an insulated window.[27] Figure 3a summarises the deformation of the crystal with the weight load upon cooling and heating (Movie 2). Surprisingly, the crystal bent during cooling from 298 to 265 K, indicating that the crystal softens as the temperature decreases. This behaviour is unusual because typical solids harden with decreasing temperature. A further decrease in temperature from 265 to 251 K straightened the crystal owing to curing. The heating process induced a crystal deformation identical to that observed during the cooling process, indicating that the deformation of the crystal with changing temperature is reversible.

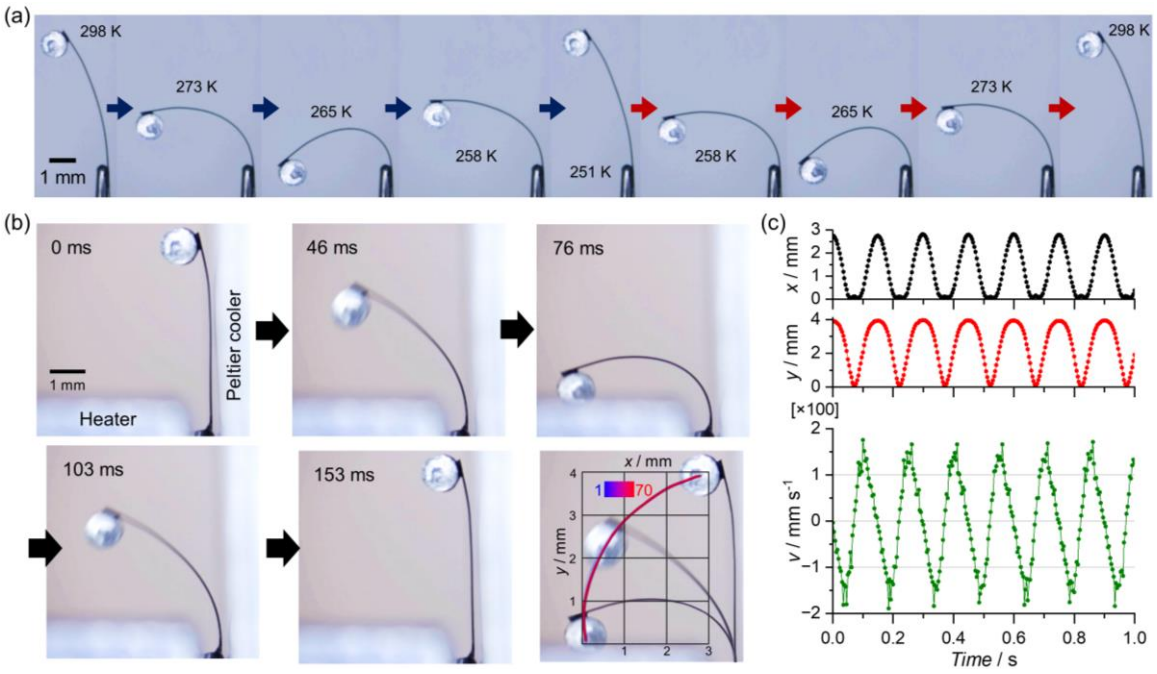

Figure 3. (a) Temperature-dependent deformation of **1** with a weight load. (b) Movement of the weight during the thermal-engine experiments. The track of the weight over 70 cycles of oscillation is depicted as a solid curve. (c) Time dependence of the *x* coordinate, *y* coordinate, and velocity (*v*) of **1** over 1 s.

Construction of the thermal engine

When **1** is loaded with a weight (1.168 mg of Al) and sandwiched between a high-temperature (34–37 °C) heat source and a low-temperature (~0 °C) heat source, a thermal engine that can extract kinetic energy from thermal energy is constructed. The crystal is ~5.2 mm long and ~43 μm thick (Figure S18). As shown in Figure 3b, the weight attached to the crystal moves with a large oscillation at a frequency of 6.84(7) Hz. When the Peltier cooler is switched on, the crystal

begins to vibrate, and the vibrations are gradually amplified until a large oscillating motion is achieved (Movie 3). This movement continues as long as the temperatures of the heat sources are maintained, and was confirmed to last for at least 160 h, corresponding to over 3.9 million cycles of bending and stretching. Unlike a previous example of molecular crystals that could extract kinetic energy from heat,[10] our crystal does not require periodic changes in temperature for actuation. Thus, to the best of our knowledge, our molecular crystal-based heat engine is the first of its kind. Figures 3c and S21 summarise the time dependence of the *x* and *y* coordinates as well as the velocity (*v*) of the weight, clearly demonstrating the high reversibility of the lifting and descending cycles (Movie 4). The average time interval for the descending and lifting processes over 70 cycles was 0.146(1) s. The maximum *v* (v_{max}) of the weight was 174(9) mm s^{-1} for descending and 179(14) mm s^{-1} for lifting (Figure S23); these values are 5–6 times faster than the reported *v* of a glass bead (0.15 mg) pushed by a thermoelastic organic crystal (29 mm s^{-1}).[13]

Figure 4a summarises the thermodynamic cycle of the heat engine. As the crystal approaches the low-temperature heat source (273 K; state A), it deforms from its equilibrium position by Δq = ~5 mm (state B and Figure S19) owing to softening. Using an elastic constant *k* of 2.94 mN m^{-1} (as summarised in Figure S20), we determined the elastic energy (E_{El}) to be $k(\Delta q)^2/2$ = 37 nJ. *k* rapidly increased to 5.48 mN m^{-1} when **1** was heated by the high-temperature heat source (298 K; state C), and E_{El} increased to 69 nJ. In other words, 32 nJ of E_{El} was supplied from the thermal energy. Based on the *v* and *y* (height) of the weight, the time dependence of its kinetic energy (E_K) and potential energy owing to gravity (E_G) can be calculated as $mv^2/2$ and mgy, respectively, where *g* is the gravitational acceleration and *m* is the mass of the weight. Figure 4b summarises E_{El}, E_G, E_K, and their sum (E_T). The maximum E_{El} (~69 nJ) is greater than the maximum E_G (~45 nJ), indicating that the E_{El} stored via the temperature change is sufficient to lift the weight to its highest position (*y* = ~3.8 mm). In other words, the E_{El} supplied from the heat source is sufficiently large for the fast and continuous motion of the weight. Based on the thermal energy absorbed by **1** as the temperature is increased from 273 to 298 K (1.0 mJ, as summarised in the caption of Figure S18) and the supplied E_{El} (32 nJ), the energy conversion efficiency of our system was estimated to be 0.003%, which is similar to that of a photothermally driven crystal actuator.[30] This heat-engine behaviour is highly reproducible, and large vibrations could be observed even in crystals of low quality (bent or chipped) (Figures S25–S27 and Movies 5–8).

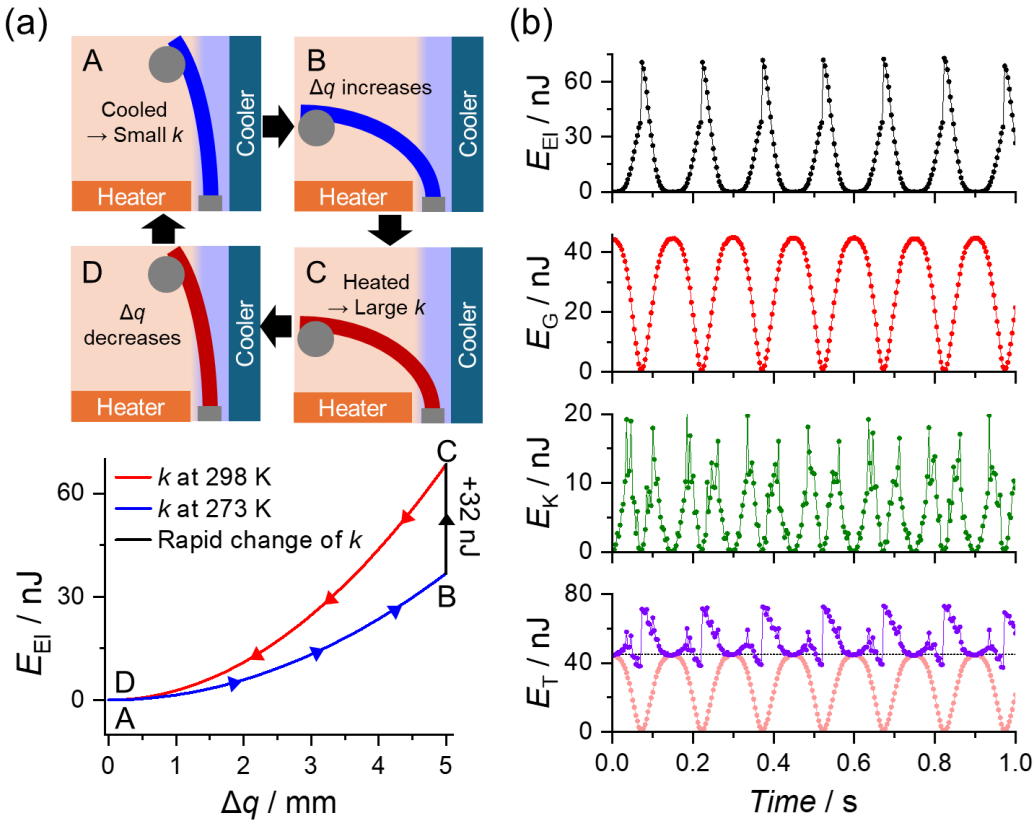

Figure 4. (a) Thermal cycle of the heat engine. (b) Time dependence of the energies of the heat engine. The potential energy owing to gravity (E_G) and maximin E_G (45 nJ) are shown in the total energy (E_T) vs. time plot as red curves and black dotted line for comparison. E_K = kinetic energy, E_{El} = elastic energy.

Microscopic mechanism of softening upon cooling

The thermal-engine behaviour of **1** is driven by changes in *k* with temperature. Notably, the temperature at which the crystal becomes most bendable (265 K in Figure 3a) is close to the boundary between the HT phase and MT state (~270 K in Figure 2b), indicating that softening is correlated with its structural changes. The following bending mechanism can be proposed based on the elongation of the crystal upon cooling (Figure 5a). (1) The weight causes the elastic crystal to arc. The outer arc is stretched, whereas the inner arc is compressed. That is, the mechanical force elongates the *a*-axis in the outer arc and compresses the *a*-axis in the inner arc. (2) When the crystal is cooled to approximately 270 K, the outer-arc region preferentially changes to the MT state with a preference for a long *a*-axis, whereas the inner-arc region remains in the HT phase with a preference for a short *a*-axis. Such an inhomogeneous structural phase transition renders the outer arc longer and the inner arc shorter, resulting in the bending of the crystal, which appears as softening, upon cooling. (3) Further decreases in temperature convert the crystal into an entirely

MT state, causing it to straighten (251 K in Figure 3a). The mechanism proposed here is identical to the operating principle of bimetals, and a similar type of curing by decreases in temperature has been reported for composite materials composed of elastic crystals, metals, and polymers.[23]

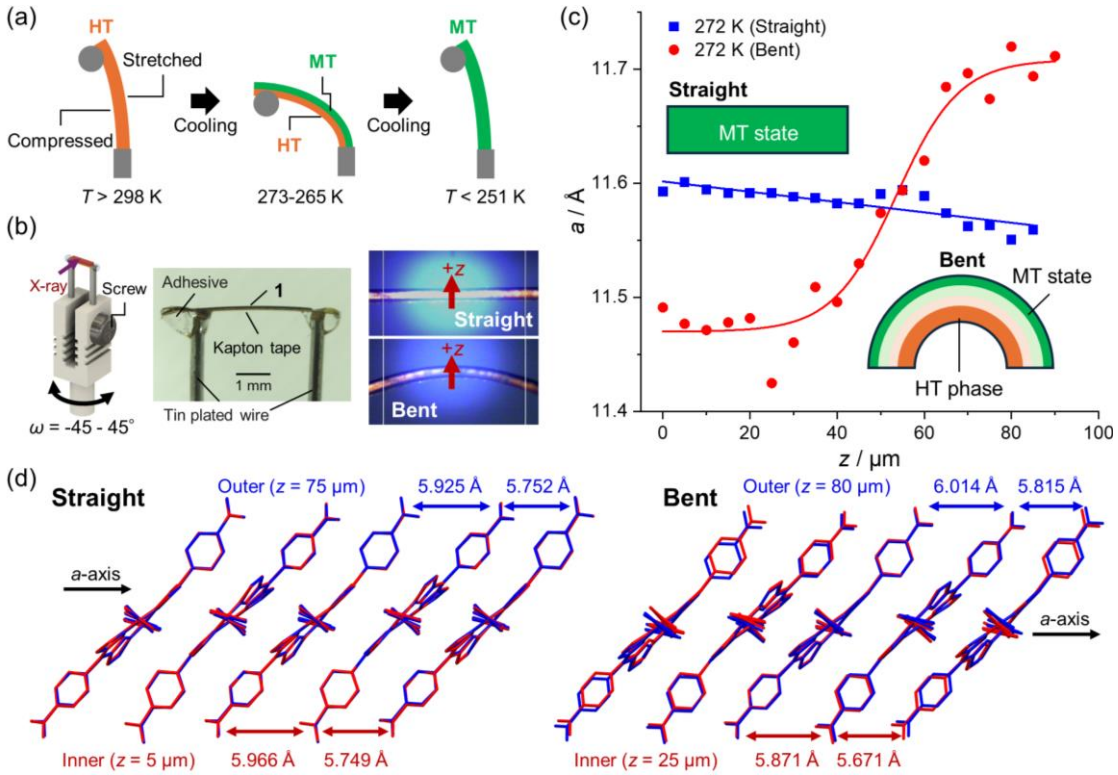

Figure 5. (a) Mechanism of the bending of the crystal based on the elongation of the *a*-axis upon cooling. (b) Experimental setup for the pinpoint X-ray structural measurements. (c) Variation in *a*-axis length as a function of the *z* position along the crystal. The solid lines represent the fits obtained using linear and sigmoidal equations. (d) Crystal structures for the inner (small *z*)- and outer (large *z*)-arc regions in the straight (left) and bent (right) configurations. The intermolecular centroid–centroid distances are shown for comparison.

To confirm the inhomogeneous structural phase transition of the crystal arc near the phase-transition temperature, we performed pinpoint X-ray structural analyses[39] of the crystal arc. Based on the crystal mount pin used to stretch crystals[40] reported by Shi *et al.*, we created a 3D model of a mount pin that could bend the crystal by adjusting a screw (Figure 5b and 3D data in the SI). The crystal was adhered to a rectangular piece of Kapton tape to prevent it from moving and fluctuating under the N_2 gas stream used for temperature control. The crystal had a straight configuration before the screw was tightened. The position of the microfocus X-ray beam (height: 2 μm; width: 4 μm) was moved from the top to the bottom of the linear crystal to scan its local

structure. The ω-scan range was restricted to −45° to 45° to avoid the X-ray irradiation of positions other than the centre of the crystal. As summarised in Figure 5c, the *a*-axis length of the straight crystal was nearly independent of the beam position and similar to that in the MT state. Tightening of the screw caused the crystal to arc. Structural mapping from the lower to the upper regions across the centre of the arc revealed that the *a*-axis length of the outer arc was approximately 1.7% longer than that of the inner arc. The longer and shorter *a*-axis lengths correspond to the MT state and HT phase, respectively, indicating that the outer- and inner-arc regions adopt the MT state and HT phase, respectively. The *z* dependence of the *a*-axis length of a bent crystal is not expressed as a linear line[24,41] but is fitted with a sigmoidal curve, indicating an inhomogeneous structural phase transition. These results are consistent with the proposed mechanism of softening upon cooling, where the outer- and inner-arc regions adopt the MT state and HT phase, respectively (Figure 5a).

Figure 5d summarises the porphyrin core structures in the inner (small *z*)- and outer (large *z*)-arc regions. The molecular structures of the outer- and inner-arc regions of the straight and bent configurations were identical, and no clear difference in the magnitudes of the thermal factors on the dodecyl chains was observed. In contrast to the molecular structures, the intracolumnar molecular distances depended on the position of the arc. In the straight configuration, the intermolecular centroid–centroid distances in the outer- and inner-arc regions were similar (Figure 5d, left). However, in the bent configuration, the intermolecular distances changed from 5.87 to 6.01 Å in the inner arc and from 5.67 to 5.81 Å in the outer arc, corresponding to a ~2.3% difference in molecular distance (Figure 5d, right). This deformation indicates that a 60 μm-thick crystal can be bent to form an arc with a diameter of 5.2 mm, indicating high flexibility.

In conclusion, we successfully constructed a molecular crystal-based thermal engine that can extract kinetic energy from ambient-temperature differences. The flexible conversion of the kinetic energy of the weight to the potential energy of crystal deformation and the rapid deformation of the crystal to accelerate the weight are crucial factors for continuous motion. The bending of the weight-loaded crystal as the temperature decreases correlates with the strain-induced phase transition associated with crystal elongation, which occurs preferentially in the outer-arc region. The mechanical properties and energy efficiency of our porphyrin-based system can be modified by changing the alkyl chain length, inserting metals, and constructing solid solutions.

Acknowledgement

This work was supported by JSPS KAKENHI grants JP23K04875 (Y.H.), JP21K14645 (Y.H.), JP20K15293 (T.K.), and JP22K14661 (Y.H.[e]). Y.H. acknowledges the financial support of The Mazda Foundation (2024). The X-ray pinpoint structural diffraction measurements were performed at the BL40XU beamline at SPring-8 (2024A1219 and 2024B1168). Y.H. wishes to thank Prof. Takashi Nakazawa (Nara Women's University) for assisting in the MALDI-TOF MS measurements.

Author contributions

H.K. performed most of the experiments and data analyses. Y.H. administered the project, conducted most of the experiments and data analyses, and wrote the manuscript. C.W., T.S., and K.I. performed the pinpoint X-ray structural measurements. Y.H.[e] and T.O. conducted the nanoindentation tests. K.Y. and S.H. performed the bending-strain measurements. M.N. and H.F. performed the DSC measurements. T.Y. and H.S. performed the heat-capacity measurements. T.K. provided the experimental equipment and financial support.

Competing interests

The authors declare no competing interests.

Materials and Correspondence

Correspondence and requests for materials should be addressed to Yoji Horii.

References

1. Camacho-Lopez, M., Finkelmann, H., Palffy-Muhoray, P. & Shelley, M. Fast liquid-crystal elastomer swims into the dark. *Nat. Mater.* **3**, 307–310 (2004).
2. Maeda, S., Hara, Y., Sakai, T., Yoshida, R. & Hashimoto, S. Self‐walking gel. *Adv. Mater.* **19**, 3480−3484 (2007).
3. Hu, W., Lum, G. Z., Mastrangeli, M. & Sitti, M. Small-scale soft-bodied robot with multimodal locomotion. *Nature* **554**, 81–85 (2018).
4. Arazoe, H. *et al.* An autonomous actuator driven by fluctuations in ambient humidity. *Nat. Mater.* **15**, 1084–1089 (2016).
5. Kobatake, S., Takami, S., Muto, H., Ishikawa, T. & Irie, M. Rapid and reversible shape changes of molecular crystals on photoirradiation. *Nature* **446**, 778–781 (2007).

6. Wie, J. J., Shankar, M. R. & White, T. J. Photomotility of polymers. *Nat. Commun.* **7**, 13260 (2016).
7. Gelebart, A. H., Vantomme, G., Meijer, E. W. & Broer, D. J. Mastering the photothermal effect in liquid crystal networks: A general approach for self-sustained mechanical oscillators. *Adv. Mater.* **29**, 1606712 (2017).
8. Ahn, C., Li, K. & Cai, S. Light or thermally powered autonomous rolling of an elastomer rod. *ACS Appl. Mater. Interfaces* **10**, 25689–25696 (2018).
9. Karothu, D. P., Weston, J., Desta, I. T. & Naumov, P. Shape-memory and self-healing effects in mechanosalient molecular crystals. *J. Am. Chem. Soc.* **138**, 13298–13306 (2016).
10. Taniguchi, T. *et al.* Walking and rolling of crystals induced thermally by phase transition. *Nat. Commun.* **9**, 538 (2018).
11. Terao, F., Morimoto, M. & Irie, M. Light-driven molecular-crystal actuators: rapid and reversible bending of rodlike mixed crystals of diarylethene derivatives. *Angew. Chem. Int. Ed Engl.* **51**, 901–904 (2012).
12. Kitagawa, D., Nishi, H. & Kobatake, S. Photoinduced twisting of a photochromic diarylethene crystal. *Angew. Chem. Int. Ed Engl.* **52**, 9320–9322 (2013).
13. Duan, Y. *et al.* Robust thermoelastic microactuator based on an organic molecular crystal. *Nat. Commun.* **10**, 4573 (2019).
14. Uddin, M. A. *et al.* Giant thermosalient effect in a molecular single crystal: Dynamic transformations and mechanistic insights. *J. Am. Chem. Soc.* (2024) doi:10.1021/jacs.4c09222.
15. Lin, J. *et al.* Mechanical Motion and Modulation of Thermal-Actuation Properties in a Robust Organic Molecular Crystal Actuator. *Adv. Funct. Mater.* **32**, 2203004 (2022).
16. Ghosh, S. & Reddy, C. M. Elastic and Bendable Caffeine Cocrystals: Implications for the Design of Flexible Organic Materials. *Angew. Chem. Int. Ed.* **51**, 10319–10323 (2012).
17. Hayashi, S. & Koizumi, T. Elastic Organic Crystals of a Fluorescent π-Conjugated Molecule. *Angew. Chem. Int. Ed.* **55**, 2701–2704 (2016).
18. Hayashi, S., Yamamoto, S.-Y., Takeuchi, D., Ie, Y. & Takagi, K. Creating elastic organic crystals of π-conjugated molecules with bending mechanofluorochromism and flexible optical waveguide. *Angew. Chem. Int. Ed Engl.* **57**, 17002–17008 (2018).
19. Kwon, T., Koo, J. Y. & Choi, H. C. Highly Conducting and Flexible Radical Crystals. *Angew. Chem. Int. Ed.* **59**, 16436–16439 (2020).
20. Yifu Chen, Zewei Chang, Jiaxing Zhang, Prof. Dr. Junbo Gong. Bending for Better: Flexible Organic Single Crystals with Controllable Curvature and Curvature-Related Conductivity for Customized Electronic Devices. *Angew. Chem. Int. Ed.*
21. Liu, H., Lu, Z., Zhang, Z., Wang, Y. & Zhang, H. Highly Elastic Organic Crystals for Flexible

Optical Waveguides. *Angew. Chem. Int. Ed.* **57**, 8448–8452 (2018).

22. Rohullah, M., Pradeep, V. V., Singh, S. & Chandrasekar, R. Mechanically controlled multifaceted dynamic transformations in twisted organic crystal waveguides. *Nat. Commun.* **15**, 4040 (2024).
23. Yang, X. *et al.* Electrically conductive hybrid organic crystals as flexible optical waveguides. *Nat. Commun.* **13**, 7874 (2022).
24. Worthy, A. *et al.* Atomic resolution of structural changes in elastic crystals of copper(II) acetylacetonate. *Nat. Chem.* **10**, 65–69 (2018).
25. Kenny, E. P., Jacko, A. C. & Powell, B. J. Mechanomagnetics in Elastic Crystals: Insights from [Cu(acac)2]. *Angew. Chem. Int. Ed.* **58**, 15082–15088 (2019).
26. Yang, X. *et al.* Remote and precise control over morphology and motion of organic crystals by using magnetic field. *Nat. Commun.* **13**, 2322 (2022).
27. Kato, H., Horii, Y., Noguchi, M., Fujimori, H. & Kajiwara, T. Molecular elastic crystals exhibiting slow magnetic relaxations. *Chem. Commun.* **59**, 14587–14590 (2023).
28. Hao, Y. *et al.* Azobenzene crystal polymorphism enables tunable photoinduced deformations, mechanical behaviors and photoluminescence properties. *J. Mater. Chem. C Mater. Opt. Electron. Devices* **9**, 8294–8301 (2021).
29. Peng, J. *et al.* Mechanical effects of elastic crystals driven by natural sunlight and force. *Angew. Chem. Int. Ed Engl.* **62**, (2023).
30. Hagiwara, Y. *et al.* Photothermally induced natural vibration for versatile and high-speed actuation of crystals. *Nat. Commun.* **14**, 1354 (2023).
31. Zheng, X. *et al.* Multi-Stimuli-Induced Mechanical Bending and Reversible Fluorescence Switching in a Single Organic Crystal. *Angew. Chem. Int. Ed.* **61**, e202113073 (2022).
32. Ghosh, S., Mishra, M. K., Ganguly, S. & Desiraju, G. R. Dual Stress and Thermally Driven Mechanical Properties of the Same Organic Crystal: 2,6-Dichlorobenzylidene-4-fluoro-3-nitroaniline. *J. Am. Chem. Soc.* **137**, 9912–9921 (2015).
33. Hasija, A. *et al.* Tracing shape memory effect and elastic bending in a conformationally flexible organic salt. *J. Mater. Chem. C Mater. Opt. Electron. Devices* **10**, 4257–4267 (2022).
34. Tong, F., Kitagawa, D., Bushnak, I., Al-Kaysi, R. O. & Bardeen, C. J. Light-powered autonomous flagella-like motion of molecular crystal microwires. *Angew. Chem. Int. Ed Engl.* **60**, 2414–2423 (2021).
35. Hoshino, N. & Akutagawa, T. Large electric piezoresistance of the flexible molecular semiconductive crystal Q(TCNQ)2 during bending. *CrystEngComm* **24**, 5234–5237 (2022).
36. Hayashi, S. *et al.* Anisotropic Poisson Effect and Deformation-Induced Fluorescence Change of Elastic 9,10-Dibromoanthracene Single Crystals. *Angew. Chem. Int. Ed.* **59**, 16195–16201 (2020).

37. Liu, H., Ye, K., Zhang, Z. & Zhang, H. An Organic Crystal with High Elasticity at an Ultra-Low Temperature (77 K) and Shapeability at High Temperatures. *Angew. Chem. Int. Ed.* **58**, 19081–19086 (2019).

38. Tang, S., Ye, K. & Zhang, H. Integrating low‐temperature‐resistant two‐dimensional elastic‐bending and reconfigurable plastic‐twisting deformations into an organic crystal. *Angew. Chem. Weinheim Bergstr. Ger.* **134**, (2022).

39. Yasuda, N. *et al.* X-ray diffractometry for the structure determination of a submicrometre single powder grain. *J. Synchrotron Radiat.* **16**, 352–357 (2009).

40. Mei, L. *et al.* Molecular Spring-like Triple-Helix Coordination Polymers as Dual-Stress and Thermally Responsive Crystalline Metal–Organic Materials. *Angew. Chem. Int. Ed.* **59**, 16061–16068 (2020).

41. Wei, C. *et al.* Atomic-resolved hierarchical structure of elastic π-conjugated molecular crystal for flexible organic photonics. *Chem* **8**, 1427–1441 (2022).